IEEE Access
Multidisciplinary ⋮ Rapid Review ⋮ Open Access Journal

Received September 10, 2020, accepted October 4, 2020, date of publication October 22, 2020, date of current version November 5, 2020.

Digital Object Identifier 10.1109/ACCESS.2020.3032904

Design of a Novel Low-Cost Consequent-Pole Permanent Magnet Synchronous Machine

WENPING CHAI[1,2], (Student Member, IEEE), ZHEN CAI[2], BYUNG-IL KWON[2], (Senior Member, IEEE), AND JUNG-WOO KWON[2], (Member, IEEE)

[1]School of New Energy, Harbin Institute of Technology at Weihai, Weihai 264209, China
[2]Department of Electronic Engineering, Hanyang University, Ansan 15588, South Korea

Corresponding authors: Jung-Woo Kwon (jwkonwis@hanyang.ac.kr) and Byung-Il Kwon (bikwon@hanyang.ac.kr)

This work was supported in part by the National Research Foundation of Korea grant funded by the Korean Government (Ministry of Science) under Grant NRF-2020R1A2B5B01002400, and in part by the Ministry of Education and National Research Foundation of Korea through the "Leaders in INdustry-university Cooperation +" Project through the BK21PLUS Program.

ABSTRACT This article proposes a novel low-cost consequent-pole permanent magnet (CPM) synchronous machine structure, considering the reluctance torque utilization. First, a novel CPM machine with doubled salient ferromagnetic iron poles (ICP-PMSM) is proposed, featuring an N pole – iron – S pole – iron sequence to maximize the reluctance torque utilization and reduce cost. Flux barriers are integrated into the rotor structure to maintain the same magnetic rotor pole number as the conventional CPM synchronous machine (CP-PMSM). Second, for a low torque ripple, soft ferrite is used to replace part of the iron pole in the ICP-PMSM (ISCP-PMSM) to improve the air-gap flux density distribution. Furthermore, the CP-PMSM, ICP-SPMSM, and ISCP-PMSM rotors are optimized for a fair comparison. The electromagnetic performances of all the optimized machines are compared with those of a conventional surface permanent magnet synchronous machine (SPMSM). It is demonstrated that the ISCP-PMSM can obtain an almost equivalent torque and torque ripple, but with reduced PM (NdFeB) usage and cost when compared to the SPMSM.

INDEX TERMS Consequent-pole, soft ferrite, flux barrier, reluctance torque, average torque.

I. INTRODUCTION

Permanent magnet (PM) machines have been widely developed for various industrial applications, including electric vehicles [1] and household appliances [2], owing to their high efficiency, high torque, and power density. However, their high cost, due to the global shortage and unstable supply of PM materials, is a significant drawback [3]. Therefore, an increasing number of researchers are focusing on obtaining adequate output torque performances with less PM material. One popular method is to use the reluctance torque [4], [5]. In addition, consequent-pole PM machines have been proposed for improving PM utilization [6], [7].

Surface PM (SPM) machines can offer higher torque density in low-speed applications owing to their low flux leakage [8]. The $i_d = 0$ control [9] is the best and most effective control method for SPM machines. However, unlike inner PM (IPM) machines, SPM machines cannot provide high reluctance torque [10]. The reluctance torque can help motors reduce the amount of PM material used while maintaining a constant total output torque. However, in conventional IPM machines, the MTPA control [11] should replace the $i_d = 0$ control for utilizing the reluctance torque; this is because the maximum output torque cannot be achieved at the zero-phase current angle. Rotor asymmetry [12] was introduced to make full use of the reluctance torque at the zero-phase current angle and improve the machine performance.

In [13], a PM machine with a dovetailed consequent-pole rotor was proposed to reduce the volume of PM material and sleeve cost, while the average torque and efficiency can be improved owing to the reduced air-gap reluctance. In [14], two novel CP-PMSM structures were presented to eliminate unipolar leakage flux in the conventional CP-PMSM. Hybrid PM machines were proposed, in which the tangential magnetized PMs were embedded into the two novel CP-PMSMs to suppress the subharmonics of the air-gap flux density in the proposed CP-PMSM and therefore enhance the output torque and reduce torque ripple. In [15], a novel CP-PMSM, featuring N-S-iron sequences, was presented to enhance the output torque and efficiency. Flux barriers were employed to

The associate editor coordinating the review of this manuscript and approving it for publication was Bo Pu.

This work is licensed under a Creative Commons Attribution 4.0 License. For more information, see https://creativecommons.org/licenses/by/4.0/

improve the magnetic symmetry and reduce the saturation of the stator yoke. However, no research has attempted to utilize the reluctance torque. In addition, conventional CP-PMSMs suffer from large torque ripple [16], predominantly due to the air-gap flux density asymmetry in the consequent poles [17].

The choice of materials is another significant aspect that affects motor performance. In general, the stator and rotor core use silicon steel sheets when assembling the PM motor. Occasionally, soft ferrite is used in high-speed PM motors [18], considering its characteristics of high permeability, high resistivity, and low loss of soft ferrite in a high-frequency alternating magnetic field; this helps to improve the electronic equipment efficiency and eliminate noise. Nevertheless, the magnetic saturation point of soft ferrite is approximately 0.5 T [19]. If it is applied to both the stator and rotor well, the torque density must be low. However, owing to this characteristic, using it in the motor core can help equalize the magnetic density distribution.

In this study, the use of PM torque and reluctance torque in CPM machines is first proposed for maximizing the output torque at the zero-phase current angle; the torque performance can be further improved by using soft ferrite instead of part of the iron pole. The remainder of this article is organized as follows. Section II first describes the working principle of the proposed topologies and performance improvement in detail; it is then applied to an actual conventional SPMSM, conventional CP-PMSM, the proposed ICP-PMSM, and the proposed ISCP-PMSM. In Section III, the rotor parameters of each investigated machine are analyzed and optimized for a fair comparison. In Section VI, the electromagnetic performances of all the investigated machines are simulated and compared. Finally, conclusions are presented in Section V.

II. FEASIBLE PRINCIPLE OF DIFFERENT TOPOLOGIES

A. GENERAL CHARACTERISTICS OF CONVENTIONAL SPMSM AND CP-PMSM

A conventional SPMSM and CP-PMSM are adopted as reference models, as shown in Figure 1 (a) and (b), respectively. They share the same stator but different rotors. The magnetization direction of the rotor PMs adopts radial. The main specifications are listed in Table I.

To analyze the working principles, the analytical model is based on the following assumptions [20]:

1) The permeance of the rotor and stator iron core is infinite.
2) The relative recoil permeability of the PMs is the same as that of the air-gap.
3) The flux leakage and end effect are neglected.

In a conventional SPMSM, the magnetic flux paths are composed of N and S PM poles, with opposite polarities, which constitute two magneto-motive force (MMF) sources and the reluctance of each part. The magnetic circuit of a conventional SPMSM is shown in Figure 2.

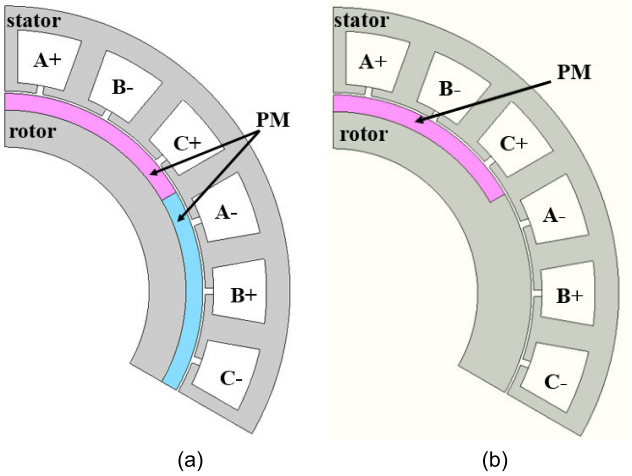

FIGURE 1. Structure of the investigated machines with conventional rotors. (a) Conventional SPMSM (b) Conventional CP-PMSM.

TABLE 1. Specifications of the conventional machine.

Item	Unit	Value
Slot / pole	-	18 / 6
Stator outer diameter	mm	170
Stator inner diameter	mm	119.4
Rotor outer diameter	mm	118
Thickness of magnet	mm	5
Stack length	mm	50
Air-gap length	mm	0.7
Turns of winding	-	417
Material of stator and rotor core	-	50H470
Material of magnet	-	Bonded NdFeB
Residual magnetic flux density of magnet material	T	0.4
Rated speed	r/min	1800

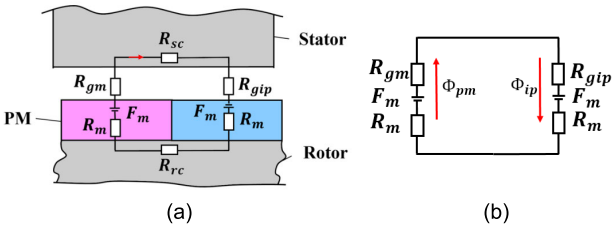

FIGURE 2. Conventional SPMSM (a) magnetic circuits (b) simplified magnetic circuits.

In the simplified MEC modeling of a conventional SPMSM, the air-gap flux in each magnetic pole can be obtained by the following:

$$\varphi_g = \frac{2F_m}{2R_m + R_{gm} + R_{gip} + R_{sc} + R_{rc}} \approx \frac{2F_m}{2R_m + R_{gm} + R_{gip}} \quad (1)$$

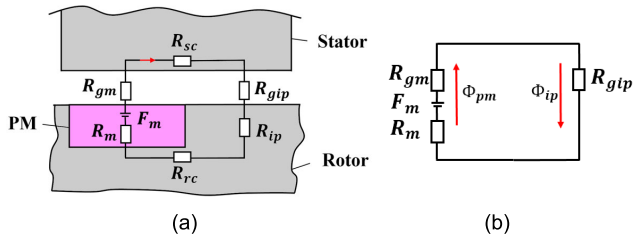

FIGURE 3. Conventional CPMSM (a) magnetic circuits (b) simplified magnetic circuits.

where F_m is the MMF generated by the PM pole, R_m is the magnetic reluctance of the PM, and R_{gm} and R_{gip} are the magnetic reluctances of the air-gap facing the PM and iron pole, respectively. R_{sc} and R_{rc} are the reluctances of the stator and rotor core, respectively, which can be neglected in the simplified magnetic model.

There is no difference in inductance between the d- and q-axis for the conventional SPMSM; therefore, no reluctance torque is generated. The torque equation is expressed as:

$$T_e = \frac{3p}{2}\left[\Lambda_{pm} i_q\right] \tag{2}$$

where p is the number of pole pairs, Λ_{pm} is the peak fundamental value of the rotor flux linking the stator windings, and i_q is the peak value of the phase current. Hence, $i_d = 0$ control is commonly utilized for conventional SPMSMs, as the most low-cost and effective method.

For the conventional CP-PMSM, all the N - or S-pole PMs are replaced by salient ferromagnetic iron, providing the magnetic flux path for the remaining PMs. Hence, the number of PMs in the conventional CP-PMSM is half of that in the SPMSM; i.e., the MEC of a pair of poles only consists of a single PM to form an MMF source. Figure 3 shows the simplified magnetic circuit model.

Similarly, the air-gap flux of each pole in the conventional CP-PMSM can be obtained as follows:

$$\begin{aligned} \varphi_{gcp} &= \frac{F_m}{R_m + R_{gm} + R_{gip} + R_{sc} + R_{rc}} \\ &\approx \frac{F_m}{R_m + R_{gm} + R_{gip}} \end{aligned} \tag{3}$$

From the comparison of air-gap flux between the conventional SPMSM and CP-SMSM in (1) and (3), it can be determined that the MMF of CP-PMSM is reduced by half and the reluctance of the PM is reduced by half accordingly. Owing to R_{gm} and R_{gip}, the reduction of MMF caused by the reduction of PM consumption will not lead to a proportional reduction in the air-gap flux; i.e., the output performance will not be significantly proportional. This explains why consequent-pole motors can increase PM utilization.

Owing to the rotor salient ferromagnetic pieces [21], the consequent pole rotor structure exploits the reluctance torque and thus increases the torque density [22]. The torque equation is expressed as:

$$T_e = \frac{3p}{2}\left[\Lambda_{pm} i_q + \left(L_d - L_q\right) i_d i_q\right] \tag{4}$$

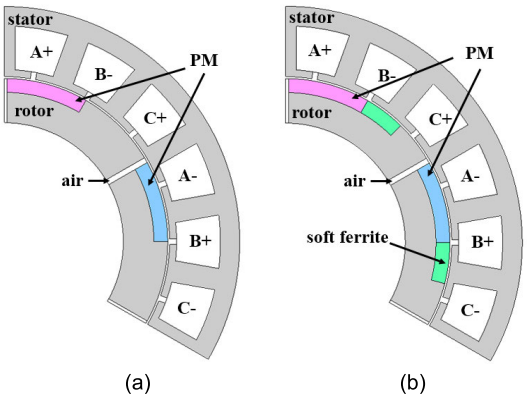

FIGURE 4. Structure of the investigated machines with proposed rotors. (a) Proposed ICP-PMSM (b) Proposed ISCP-PMSM.

where L_d and L_q are the inductances of the d- and q-axes, respectively, and $i_d = -i_s sin(\delta)$ and $i_q = i_s cos(\delta)$ are the currents of the d- and q-axes, respectively. i_s is the peak value of the phase current. δ is the spatial angle of the stator current vector, measured with respect to the q-axis, also referred to as the current phase angle. However, when the consequent-pole motors are controlled by $i_d = 0$ control, the torque equation should be the same as in (2), indicating that the reluctance torque cannot be utilized.

B. PERFORMANCE IMPROVEMENT IN THE PROPOSED ICP-PMSM AND ISCP-PMSM

To utilize the reluctance torque produced by the salient ferromagnetic pieces in CP-PMSM under $i_d = 0$ control, an ICP-PMSM with doubled salient ferromagnetic iron poles is proposed, as shown in Figure 4 (a). The magnet shape, number of poles, and stator of the proposed model are consistent with those of the conventional CPMSM. The air-gap flux barriers in the ICP-PMSM are used to prevent that flux flows from one PM to another with opposite polarity. The main specifications are the same as those in Table I.

Figure 5 shows the magnetic circuit of the ICP-PMSM. R_b represents the reluctance of the air-gap flux barrier; ϕ'_{pm} and ϕ'_{ip} represent the air-gap flux located above the PM pole and iron pole, respectively; and ϕ'_{pm} and ϕ'_{ip} represent the air-gap flux located above the other PM pole and iron pole, respectively.

When R_b is large enough, the air-gap flux in each PM and iron pole should be equal, expressed as follows:

$$\phi_{pm} = \phi_{ip} = \phi'_{pm} = \phi'_{ip} \approx \frac{F_m}{R_m + R_{gm} + R_{gip}} \tag{5}$$

The magnetic reluctance of the air barrier can be calculated by:

$$R_b = \frac{l_b}{\mu_0 \mu_r A_b} \tag{6}$$

where μ_0 is the magnetic permeability of vacuum, μ_r is the relative magnetic permeability of air, A_b is the cross-sectional area of the air barrier, and l_b is the width of the air barrier.

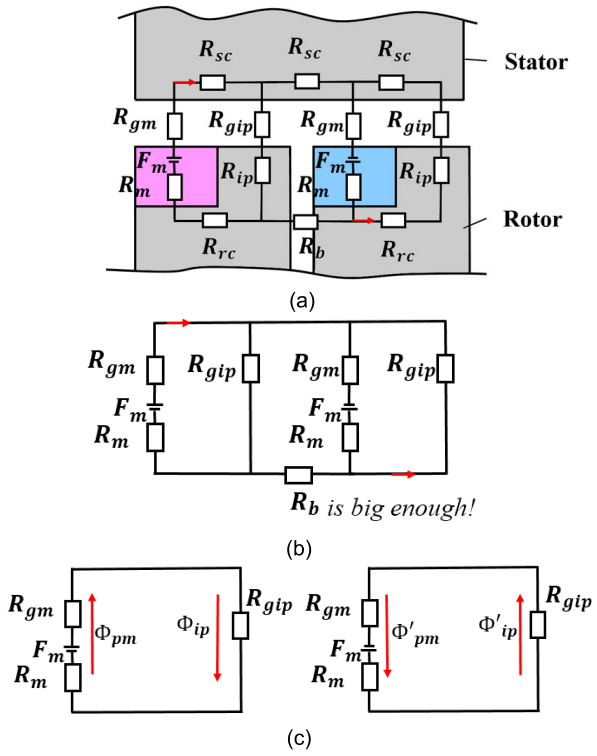

FIGURE 5. Proposed ICP-PMSM (a) magnetic circuits (b)simplified magnetic circuits (c) simplified magnetic circuits when R_b is sufficiently large.

Therefore, if the air-gap flux barrier is sufficiently wide, the air-gap flux of the ICP-PMSM will match that of a conventional CP-PMSM, indicating that the PM torque of the conventional CP-PMSM is equal to that of the ICP-PMSM. However, if the air-gap flux barrier is too wide, the equivalent operating air-gap length will increase, reducing the output torque. Hence, the width of the air-gap flux barrier (l_b), as a key parameter, should be designed carefully.

Conventionally, for PM torque, the d-axis is aligned with the rotor flux linkage phasor, depending on the direction of the total rotor magnetic flux. The q-axis is counterclockwise perpendicular to the d-axis. The d-q axis of the reluctance torque should be changed, referred to as the dr-qr axis, owing to the double salient ferromagnetic iron poles. The d-q axis of the PM torque and the reluctance torque of the ICP-PMSM are shown in Figure 6. The angle difference between the d-q axis and dr-qr axis is 45 °, whereas it should be 90 ° in the general torque equation.

Therefore, the torque equation of the ICP-PMSM should be expressed as:

$$T_e = \frac{3p}{2}\left[\Lambda_{pm} i_s \cos\delta + 0.5\left(L_d - L_q\right) i_s^2 \sin 2\left(\delta + 45\right)\right] = \frac{3p}{2}\left[\Lambda_{pm} i_s \cos\delta + 0.5\left(L_d - L_q\right) i_s^2 \cos 2\delta\right] \quad (7)$$

When the phase current is zero, the output torque can be maximized by fully using the magnetic and reluctance torque. When the proposed ICP-PMSM uses $i_d = 0$ control,

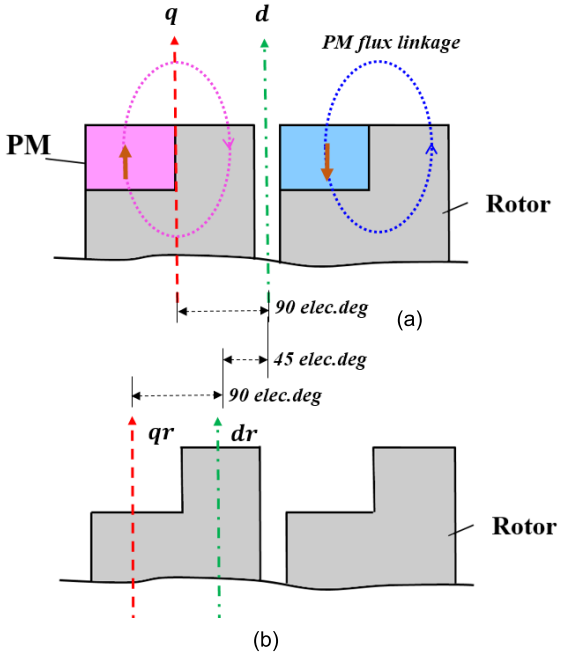

FIGURE 6. d-q axis in ICP-PMSM (a) PM torque (b) reluctance torqu.

the torque equation (7) demonstrates that full use can be made of the PM and reluctance torque.

The ICP-PMSM suffers the same magnetic imbalance issue as the conventional CP-SMSM. Therefore, soft ferrite with a low magnetic saturation point replaces part of the iron consequent pole for alleviating the magnetic imbalance to improve output performance, which is referred to as ISCP-PMSM. The rotor structure of ISCP-PMSM features N-soft ferrite-iron-S-soft ferrite-iron sequences, as shown in Figure 4 (b).

The permeability of soft ferrite is slightly smaller than that of iron, so the air-gap flux equation of ISCP-PMSM can be considered the same as that of ICP-PMSM. Normally, the magnetic saturation point of iron (e.g., 50H470) is approximately 1.8 T and the magnetic saturation point of soft ferrite (e.g., PC95_80deg) is approximately 0.44 T, as shown in Figure 7.

It is well known that magnetic flux can no longer increase when it reaches the saturation point of the material. As part of the iron is replaced by soft ferrite in the consequent pole, the magnetic flux close to the PM in the consequent pole is limited to 0.44 T and the extra magnetic flux disperses to the far side of the PM, which can make the magnetic flux density distribution uniform. Diagrams of the magnetic flux distribution in the pole of the ICP-PMSM and ISCP-PMSM are shown in Figure 8. Therefore, the torque performance can be improved.

Figure 9 (a) and (b) show the slotless magnetic flux density distribution of the proposed ICP-PMSM and ISCP-PMSM, respectively. It can be observed that the ICP-PMSM inherits the asymmetric air-gap flux density of the CP topology and the ISCP-PMSM can effectively suppress the asymmetric air-gap flux density.

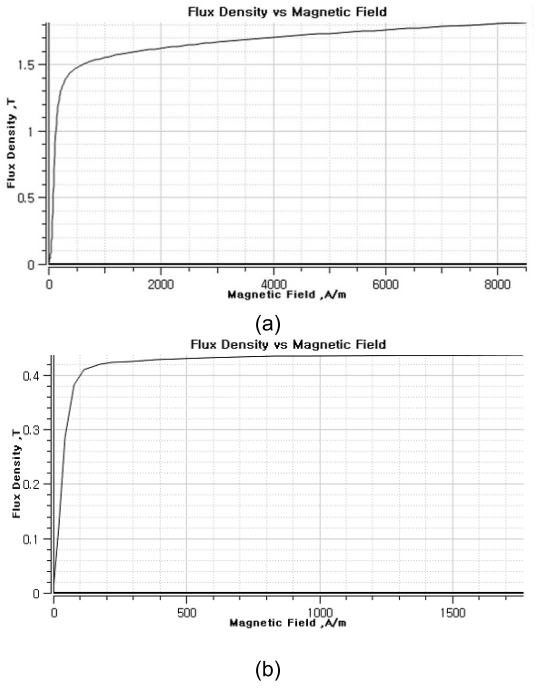

FIGURE 7. B-H curve comparison (a) iron core (50H470) (b) soft ferrite (PC95_80deg).

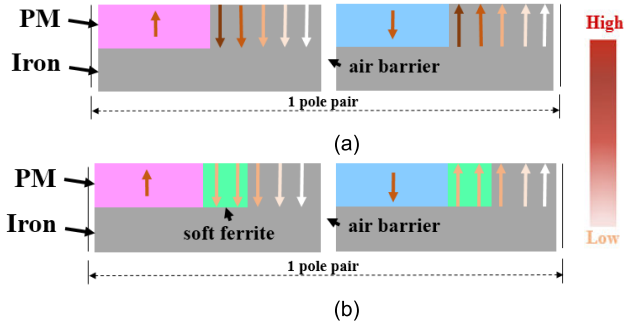

FIGURE 8. Diagram of magnetic flux distribution (a) pole of ICP-PMSM (b) pole of ISCP-PMSM.

III. OPTIMIZATION DESIGN OF ROTORS

For a fair comparison, all the investigated machines share the same stator and the thickness of the PM is fixed at 5 mm. The rotor of a conventional SPMSM adopts a full PM arc. The output average torque is 7.35 Nm and its torque ripple is 20.06 %. To match the output performance of the conventional SPMSM, the rotors of CP-PMSM, ICP-PMSM, and ISCP-PMSM are optimized via FE analysis, under the constraints of equal copper loss.

A. OPTIMIZATION DESIGN OF THE CP-PMSM ROTOR

The PM-arc ratio is defined as

$$\alpha_p = \frac{\theta_{pm} * p}{2\pi} \tag{8}$$

where p and θ_m are the number of pole pairs and PM arc angle of the PM machine, respectively.

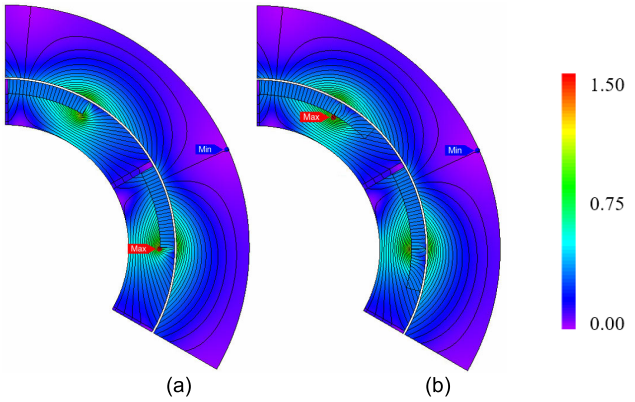

FIGURE 9. Slotless magnetic flux density distribution (a) ICP-PMSM (b) ISCP-PMSM.

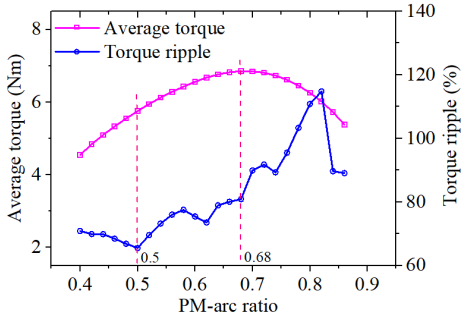

FIGURE 10. Average torque and torque ripple with variable α_p.

It is demonstrated that the maximum output torque of a conventional CP-PMSM can be obtained by optimizing the PM-arc ratio [3], [23].

It can be seen that the machine can obtain the maximum output torque at $\alpha_p = 0.68$ and the minimum torque ripple at $\alpha_p = 0.5$; this is due to the increase in air-gap flux density asymmetry when $\alpha_p > 0.5$, which is concluded based on the principle that the same flux flows through the PM and iron pole of the CP-PMSM ($\Phi_{pm} = \Phi_{ip}$) [24]. From Figure 10, it can be seen that the maximum output torque and torque ripple of the conventional CP-PMSM cannot reach that of a conventional SPMSM.

B. OPTIMIZATION DESIGN OF THE ICP-PMSM ROTOR

For ICP-PMSM, the PM-arc ratio α_p and air barrier width b are complex for maximizing the output torque, so an optimal design using the Kriging method and a genetic algorithm (GA) is to be performed [25]. The objective function is to achieve the same output torque as the conventional SPMSM in an ICP-PMSM.

1) Objective functions:
   Average torque = 0.735 Nm
   Minimum PM Volume
2) Constraints:
   Average torque = 0.735 Nm
3) Design variables:
   $0.8 < b < 4$
   $0.4 < \alpha_p < 0.8$

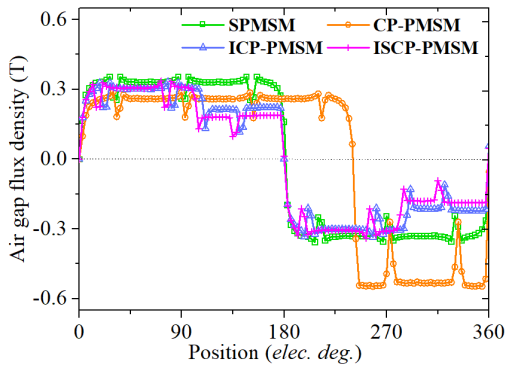

FIGURE 11. Air-gap flux density distribution of investigated machines.

The optimal design results were obtained via the GA as $b = 1.423$ mm and $\alpha_p = 0.6275$.

C. OPTIMIZATION DESIGN OF THE ISCP-PMSM ROTOR

The soft ferrite-arc ratio β_s is defined as

$$\beta_s = \frac{\theta_{softferrite}}{\frac{2\pi}{p}\left(1-\alpha_p\right) - \frac{b}{R}} \tag{9}$$

where $\theta_{softferrite}$ is the soft ferrite-arc angle of the PM machine and R is the radius of the rotor core.

For ISCP-PMSM, there is an optimal PM-arc ratio, α_p, air barrier width, b, and soft ferrite-arc ratio, β_s, for maximizing the output torque. The same optimizing process is applied to the ISCP-PMSM.

1) Objective functions:
   Average torque = 0.735 Nm
   Minimum PM Volume and torque ripple
2) Constraints:
   Average torque = 0.735 Nm
3) Design variables:
   $0.8 < b < 4$
   $0.4 < \alpha_p < 0.8$
   $0 < \beta_s < 1$

The optimal design results are obtained via the GA as $b = 1.20$ mm, $\alpha_p = 0.592$, and $\beta_s = 0.770$.

IV. ELECTROMAGNETIC PERFORMANCE COMPARISON AND ANALYSIS

To verify the effectiveness of the ISCP-PMSM proposed in the previous section, the electromagnetic performance of the ISCP-PMSM is investigated and compared to those of the conventional SPMSM, conventional CP-PMSM, and proposed ICP-PMSM.

A. AIR-GAP FLUX DENSITY WITH NO LOAD

Figure 11 shows the air-gap flux density distribution of the conventional SPMSM and CP-PMSM, as well as the ICP-PMSM and ISCP-PMSM with a no-load condition. It can be seen that the air-gap flux density distribution of the conventional CP-PMSM is asymmetrical, which will cause more torque ripple; this is due to the air-gap flux in one pole pair being produced by one PM pole and flowed by one iron pole. However, the structure of pole pairs featuring N-iron-S-iron sequences in the ICP-PMSM, and N-soft ferrite-iron-S-soft ferrite-iron sequences in the ISCP-PMSM, can effectively improve the air-gap flux density by fixing the rotor pole pitch.

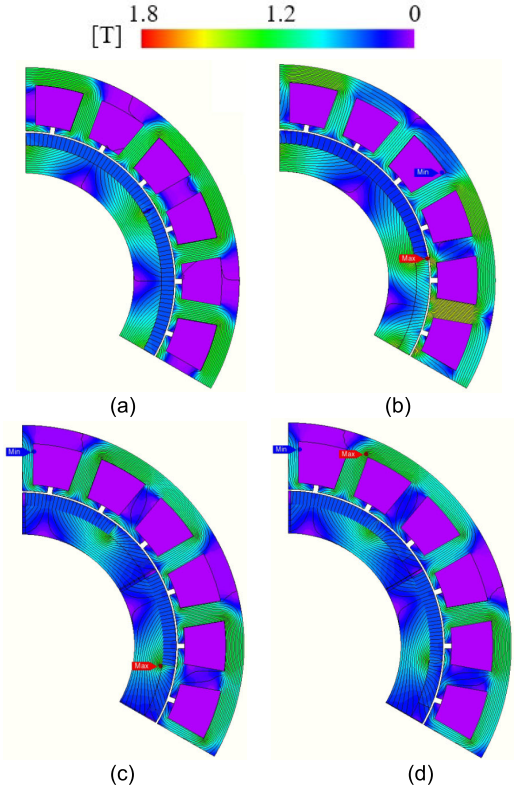

FIGURE 12. Magnetic flux density distribution (a) conventional SPMSM (b) conventional CP-PMSM (c) ICP-PMSM (d) ISCP-PMSM.

The magnetic flux density distributions from the study in FEM for the conventional SPMSM, conventional CP-PMSM, and ISCP-PMSM are shown in Figure 12. It can be observed that a lower flux density exists in the ICP-PMSM and ISCP-PMSM, compared to that in the conventional SPMSM and CP-PMSM. This is predominantly due to lower PM usage. The air barrier in the ICP-PMSM and ISCP-PMSM helps the flux generated by the PM to more easily flow through the iron pole for higher torque production. Meanwhile, it can be noted that the conventional CP-PMSM and ICP-PMSM are more likely to reach a high flux density distribution in the section of the iron pole near the PM. Figure 12 (d) shows that the use of soft ferrite can help to make the magnetic flux density distribution uniform, confirming the supposition in Figures 8 and 9.

B. BACK-EMF

The simulated back-EMFs and their FFT results are presented in Figure 13 (a) and (b), respectively, for the conventional SPMSM, conventional CP-PMSM, ICP-PMSM, and ISCP-PMSM. It can be seen that the conventional SPMSM and CP-PMSM have a larger fundamental back-EMF owing

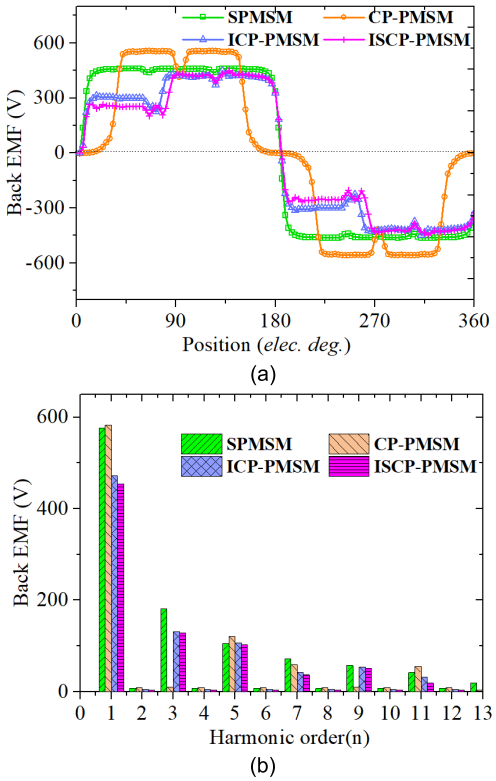

FIGURE 13. Back-EMF of the investigated machines (a) waveform (b) FFT.

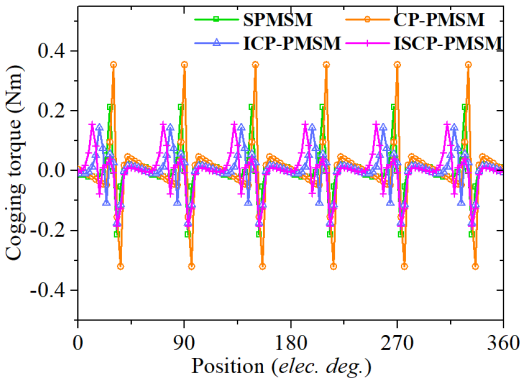

FIGURE 14. Variation of cogging torque with rotor positions.

to the larger air-gap flux density. The CP-PMSM lacks the 3rd and 9th harmonics compared to the conventional SPMSM, while the ICP-PMSM and ISCP-PMSM are rich in odd harmonics, similar to conventional SPMSMs. Previous research [26] has proven that the 3rd harmonic is beneficial to the average output torque.

C. TORQUE PERFORMANCE

The cogging torque of the four investigated motors is shown in Figure 14 and their peak-to-peak values are listed in Table II. The peak-to-peak value of the cogging torque of the CP-PMSM is the largest, while those of the ICP-PMSM and ISCP-PMSM are much smaller.

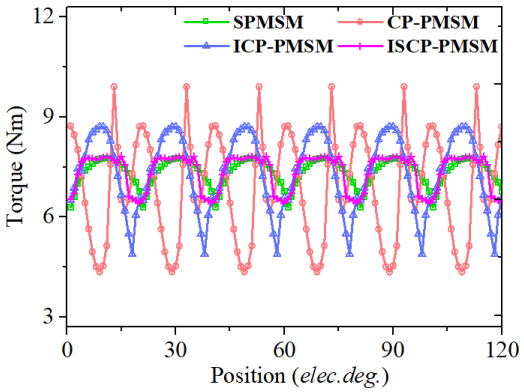

FIGURE 15. Variation of output torque with rotor positions.

TABLE 2. Performance comparison.

Item	Unit	SPMSM	CP-PMSM	ICP-PMSM	ISCP-PMSM
Back-EMF (RMS)	V	443.07	430.07	361.06	347.15
Cogging torque	Nm	0.428	0.674	0.319	0.342
Total torque	Nm	7.350	6.852	7.335	7.357
PM torque	Nm	7.350	6.685	5.433	5.527
Reluctance torque	Nm	0	0.167	1.902	1.83
Torque ripple	%	20.06	80.89	52.12	19.08
PM-arc ratio	--	1	0.68	0.63	0.59
PM utilization ratio	Nm/cm^3	0.083	0.114	0.131	0.141
Rotor cost	$	48.3	34.2	31.0	29.8
Efficiency	%	93.6	91.0	91.1	92.7

The variations in electromagnetic torque for the four investigated machines under $i_d = 0$ control are illustrated in Figure 15 and their characteristics are listed in Table II. It can be seen that the ISCP-PMSM can achieve a similar average output torque and torque ripple to the conventional SPMSM, while the conventional CP-PMSM cannot and the ICP-PMSM can only achieve a similar average output torque but a higher torque ripple. To provide useful insight into the relevance of these results, the frozen permeability method [27] was used to separate the output torque into PM torque and reluctance torque. It can be observed that the structure of the ICP-PMSM and ISCP-PMSM can be beneficial to reluctance torque production at the zero phase current angle, while there is almost zero in the conventional SPMSM and ICP-PMSM. Compared to the ICP-PMSM, the ISCP-PMSM obtains a slightly smaller reluctance torque owing to the lower relative permeability of soft ferrite compared to iron. The ISCP-PMSM can achieve a slightly higher PM torque and a much lower torque ripple, which is mostly due to the improved air-gap flux density. From the perspective of PM usage, the ISCP-PMSM can only use 59 % of that in the conventional SPMSM. Under the same control method, PM material is one of the primary costs of motor manufacturing. A lower PM material usage corresponds to a lower cost.

The PM utilization ratio (average torque per PM volume) is effectively improved by 57.8% and 69.9% for the ICP-PMSM and ICSP-PMSM, respectively, compared to that of the conventional SPMSM. The conventional SPMSM and the ICSP-PMSM exhibit similar efficiencies.

V. CONCLUSION

In this article, a novel CP-PMSM, with a combination of iron and soft ferrite, is proposed to achieve adequate torque performance with reduced PM usage and cost. First, based on the conventional SPMSM, the CP-PMSM is presented. However, regardless of the PM-arc ratio, the average torque and torque ripple cannot reach that of a conventional SPMSM. Second, the ICP-PMSM was proposed and optimized using the reluctance torque. Although the average torque can be satisfied, the torque ripple is still high. Finally, the ISCP-PMSM was proposed and optimized, which shows a satisfactory output performance; i.e., the average torque and torque ripple of the proposed ISCP-PMSM at zero phase current are similar, indicating that the proposed machine can completely replace the conventional SPMSM at a lower cost.

REFERENCES

[1] K. T. Chau, C. C. Chan, and C. Liu, "Overview of permanent-magnet brushless drives for electric and hybrid electric vehicles," *IEEE Trans. Ind. Electron.*, vol. 55, no. 6, pp. 2246–2257, Jun. 2008.
[2] J.-W. Kwon and B.-I. Kwon, "High-efficiency dual output stator-PM machine for the two-mode operation of washing machines," *IEEE Trans. Energy Convers.*, vol. 33, no. 4, pp. 2050–2059, Dec. 2018.
[3] I. Petrov and J. Pyrhonen, "Performance of low-cost permanent magnet material in PM synchronous machines," *IEEE Trans. Ind. Electron.*, vol. 60, no. 6, pp. 2131–2138, Jun. 2013.
[4] S. Ooi, S. Morimoto, M. Sanada, and Y. Inoue, "Performance evaluation of a high-power-density PMASynRM with ferrite magnets," *IEEE Trans. Ind. Appl.*, vol. 49, no. 3, pp. 1308–1315, May 2013.
[5] Q. Chen, Y. Yan, G. Liu, and G. Xu, "Design of a new fault-tolerant permanent magnet machine with optimized salient ratio and reluctance torque ratio," *IEEE Trans. Ind. Electron.*, vol. 67, no. 7, pp. 6043–6054, Jul. 2020.
[6] S.-U. Chung, J.-W. Kim, Y.-D. Chun, B.-C. Woo, and D.-K. Hong, "Fractional slot concentrated winding PMSM with consequent pole rotor for a low-speed direct drive: Reduction of rare Earth permanent magnet," *IEEE Trans. Energy Convers.*, vol. 30, no. 1, pp. 103–109, Mar. 2015.
[7] S.-U. Chung, J.-W. Kim, B.-C. Woo, D.-K. Hong, J.-Y. Lee, and D.-H. Koo, "A novel design of modular three-phase permanent magnet Vernier machine with consequent pole rotor," *IEEE Trans. Magn.*, vol. 47, no. 10, pp. 4215–4218, Oct. 2011.
[8] K. Wang, Z. Y. Gu, Z. Q. Zhu, and Z. Z. Wu, "Optimum injected harmonics into magnet shape in multiphase surface-mounted PM machine for maximum output torque," *IEEE Trans. Ind. Electron.*, vol. 64, no. 6, pp. 4434–4443, Jun. 2017.
[9] J. Pyrhonen, V. Hrabovcova, and R. S. Semken, *Electrical Machine Drives Control: An Introduction*. Hoboken, NJ, USA: Wiley, 2016.
[10] K. I. Laskaris and A. G. Kladas, "Comparison of internal and surface permanent-magnet motor topologies for electric vehicle applications," in *Proc. 8th Int. Symp. Adv. Electromechanical Motion Syst. Electr. Drives Joint Symp.*, Jul. 2009, pp. 1–4.
[11] P. Niazi, H. A. Toliyat, and A. Goodarzi, "Robust maximum torque per ampere (MTPA) control of PM-assisted SynRM for traction applications," *IEEE Trans. Veh. Technol.*, vol. 56, no. 4, pp. 1538–1545, Jul. 2007.
[12] W. Zhao, H. Shen, T. A. Lipo, and X. Wang, "A new hybrid permanent magnet synchronous reluctance machine with axially sandwiched magnets for performance improvement," *IEEE Trans. Energy Convers.*, vol. 33, no. 4, pp. 2018–2029, Dec. 2018.
[13] J. Li, K. Wang, and C. Liu, "Torque improvement and cost reduction of permanent magnet machines with a dovetailed consequent-pole rotor," *IEEE Trans. Energy Convers.*, vol. 33, no. 4, pp. 1628–1640, Dec. 2018.
[14] K. Wang, J. Li, S. S. Zhu, and C. Liu, "Novel hybrid-pole rotors for consequent-pole PM machines without unipolar leakage flux," *IEEE Trans. Ind. Electron.*, vol. 66, no. 9, pp. 6811–6823, Sep. 2019.
[15] J. Li, K. Wang, and C. Liu, "Comparative study of consequent-pole and hybrid-pole permanent magnet machines," *IEEE Trans. Energy Convers.*, vol. 34, no. 2, pp. 701–711, Jun. 2019.
[16] G. H. Zhang, K. Wang, and J. Li, "Torque ripple suppression of consequent-pole permanent magnet machine by magnet shifting," in *Proc. 22nd Int. Conf. Electr. Mach. Syst. (ICEMS)*, Harbin, China, Aug. 2019, pp. 1–6.
[17] H. Yang, Z. Q. Zhu, H. Lin, H. Li, and S. Lyu, "Analysis of consequent-pole flux reversal permanent magnet machine with biased flux modulation theory," *IEEE Trans. Ind. Electron.*, vol. 67, no. 3, pp. 2107–2121, Mar. 2020.
[18] X. Wang, X. Zhang, S. Yan, X. Wang, and C. Zhang, "The analysis of high speed slotless permanent magnet brushless DC motor based on soft magnetic ferrite," in *Proc. Int. Conf. Electr. Mach. Syst., Incheon*, pp. 1061–1064, 2010.
[19] *Soft Ferrite Products*. Accessed: Sep. 2020. [Online]. Available: http://www.hitachi-metals.co.p/e/products/elec/tel/p13_21.html
[20] J. Li and K. Wang, "Analytical determination of optimal PM-arc ratio of consequent-pole permanent magnet machines," *IEEE/ASME Trans. Mechatronics*, vol. 23, no. 5, pp. 2168–2177, Oct. 2018.
[21] J.-X. Shen, H.-Y. Li, H. Hao, and M.-J. Jin, "A coaxial magnetic gear with consequent-pole rotors," *IEEE Trans. Energy Convers.*, vol. 32, no. 1, pp. 267–275, Mar. 2017.
[22] S.-U. Chung, S.-H. Moon, D.-J. Kim, and J.-M. Kim, "Development of a 20-pole-24-slot SPMSM with consequent pole rotor for in-wheel direct drive," *IEEE Trans. Ind. Electron.*, vol. 63, no. 1, pp. 302–309, Jan. 2016.
[23] Z. Z. Wu and Z. Q. Zhu, "Partitioned stator flux reversal machine with consequent-pole PM stator," *IEEE Trans. Energy Convers.*, vol. 30, no. 4, pp. 1472–1482, Dec. 2015.
[24] J. Li, K. Wang, F. Li, S. S. Zhu, and C. Liu, "Elimination of even-order harmonics and unipolar leakage flux in consequent-pole PM machines by employing N-S-Iron–S-N-Iron rotor," *IEEE Trans. Ind. Electron.*, vol. 66, no. 3, pp. 1736–1747, Mar. 2019.
[25] W. Chai, W. Zhao, and B.-I. Kwon, "Optimal design of wound field synchronous reluctance machines to improve torque by increasing the saliency ratio," *IEEE Trans. Magn.*, vol. 53, no. 11, pp. 1–4, Nov. 2017.
[26] R. O. C. Lyra and T. A. Lipo, "Torque density improvement in a six-phase induction motor with third harmonic current injection," *IEEE Trans. Ind. Appl.*, vol. 38, no. 5, pp. 1351–1360, Sep. 2002.
[27] G.-J. Li, G. Jewell, and Z.-Q. Zhu, "Performance investigation of hybrid excited switched flux permanent magnet machines using frozen permeability method," *IET Electr. Power Appl.*, vol. 9, no. 9, pp. 586–594, Nov. 2015.

WENPING CHAI (Student Member, IEEE) was born in Liaoning, China, in 1991. She received the B.S. degrees in electrical engineering and automation and also management from the Harbin Institute of Technology, in 2014, and the Ph.D. degree in electrical engineering from the Department of Electrical and Electronic Engineering, Hanyang University, South Korea, in 2020. She is currently an Assistant Professor of electrical engineering with the School of New Energy, Harbin Institute of Technology at Weihai, Weihai, China. Her research interest includes the design, analysis, and optimization of electric machines.

ZHEN CAI was born in Jilin, China, in 1995. He received the B.S. degree in measurement and control technology and instrumentation from the China University of Mining and Technology, Beijing, in 2017, and the M.S. degree from the Department of Mechatronics, Hanyang University, Ansan, South Korea, in 2020. His research interest includes the design, analysis, and optimization of electric machines, especially on motors.

BYUNG-IL KWON (Senior Member, IEEE) was born in 1956. He received the B.S. and M.S. degrees in electrical engineering from Hanyang University, Ansan, South Korea, in 1981 and 1983, respectively, and the Ph.D. degree in electrical engineering, machine analysis from The University of Tokyo, Tokyo, Japan, in 1989.

From 1989 to 2000, he was a Visiting Researcher with the Faculty of Science and Engineering Laboratory, University of Waseda, Tokyo. In 1990, he was a Researcher with the Toshiba System Laboratory, Yokohama, Japan. In 1991, he was a Senior Researcher with the Institute of Machinery and Materials Magnetic Train Business, Daejeon, South Korea. From 2001 to 2008, he was a Visiting Professor with the University of Wisconsin–Madison, Madison, WI, USA. He is currently a Professor with Hanyang University. His research interest includes the design and control of electric machines.

JUNG-WOO KWON (Member, IEEE) was born in 1992. He received the B.S. degrees in bio-nano engineering and electrical engineering and the M.S. and Ph.D. degrees from Hanyang University, Ansan, South Korea, in 2015 and 2019. He is currently working as a Postdoctoral Researcher with the Department of Electrical and Electronic Engineering, Hanyang University. His research interest includes electric machines, especially on motors.